J Solid State Electrochem (2017) 21:211–222
DOI 10.1007/s10008-016-3357-6

ORIGINAL PAPER

Development of copper-stabilized conducting-polymer/polyoxometalate hybrid materials for effective electrochemical charging

Lidia Adamczyk[1]

Received: 13 May 2016 / Revised: 28 July 2016 / Accepted: 5 August 2016 / Published online: 23 August 2016

Abstract A hybrid organic-inorganic material composed of poly (3,4-ethylenedioxythiophene), PEDOT, derivatized with 4-(pyrrol-e1-yl) benzoic acid, PyBA, and Keggin-type copper (II)-salt of $H_3PMo_{12}O_{40}$ has been proposed here. Such features as good electronic conductivity of PEDOT, hydrophilic and coordination capabilities of PyBA, the ability of copper (II) ions to link PyBA carboxylic groups, and phosphomolybdate anionic sites, as well as high protonic and mixed-valence conductivities of $H_3PMo_{12}O_{40}$ have been explored here to produce a stable composite material charcterized by reasonable charge propagation dynamics. Characterization and formation of the hybrid ca. 0.6 μm thick PEDOT/PyBA-$Cu_xH_yPMo_{12}O_{40}$ films have been asessed by FTIR, XRD, AFM, SEM, as well as using electrochemical methods. Among important feautures of the proposed hybrid system is the ability to undergo reversible charging/discharhging (both under voltammetric and galvanostatic conditions) in a manner analogous to what is observed in battery--type cells. Typical parameters, such as specific capacity, energy, and power densities, are provided and discussed.

Keywords Conducting polymer · Polyoxometalates · Battery · Surface modification

✉ Lidia Adamczyk
adamczyk@wip.pcz.pl

[1] Division of Chemistry, Department of Materials Processing, Technology and Applied Physics, Czestochowa University of Technology, Al. Armii Krajowej 19, PL 42-200 Czestochowa, Poland

Introduction

There has been growing recent interest in the development of electrochemical charge storage devices capable of yielding high power densities and exhibiting long-term durability. In this respect, two distinct types of devices [1–5], namely electrochemical capacitors (supercapacitors) and highly efficient battery-type systems basically exist. Contrary to the latter systems requiring true redox reactions, charge storage processes in double-layer type capacitors are non-Faradaic, and their operation involves electrostatic attraction of electrolyte ions onto large surface area electrode materials. Charge storage in secondary batteries is typically based on reversible redox reactions accompanied by insertion on repulsion of ions in bulk electrode materials. These processes are typically diffusion-controlled and, therefore, are slow enough to make such batteries low or moderate power devices. Because charge displacement in supercapacitors could be largely interfacial and no diffusional limitations there exist, they can become high power devices. To fabricate high-energy density rechargeable battery-type materials, one has to refer to fundamental concepts of fast redox transitions within thin solid films of redox-conducting materials [6–9]. Applicable systems include protonically/electronically conducting mixed valence inorganic materials (e.g., polyoxometalates of molybdenum or tungsten [10–13]) and certain organic conjugated conducting polymers (e.g., pristine or derivatized poly (3,4-ethylenedioxythiophene), PEDOT [14, 15]). Despite the three-dimensional (μm level) character of films of such materials, they should effectively exhibit the thin layer type (rather than diffusional or mixed type) behavior consistent with the systems' interfacial electrochemical reversibility. In practice, electron transfers between redox sites must fast and accompanied by unimpeded displacements of counter ions providing charge balance during redox transitions. To achieve this goal,

the applicable materials (films) should not only be porous but also contain large populations of redox facile active sites [6–8]. On practical grounds, an important issue is the system's long-term stability.

In the present work, a robust conducting polymer (PEDOT) [15] (that has been intentionally derivatized with 4-(pyrrole-1-yl) benzoic acid, or PyBA [16, 17] to improve the material's hydrophilicity and to provide carboxylate groups capable of coodinating copper (II) ions) has been considered. Furthermore, the polymer system has been combined (by linking through Cu (II) ions) with the Keggin-type polyoxometalate, phoshododecamolybdate. The latter heteropolymolybdate [10–13, 15] is known to exibit fast redox reactions facilitated by high proton mobility.

The choice of PEDOT as the applicable conducting polymer material has been dictated by its high stability, fairly low toxicity, and easy handling [18–22]. The PEDOT-based coatings may act as good charge mediators, and they are unlikely to be degraded through fouling by various reactants involved in organic redox processes. By introducing polynuclear heteropolymolybdates to the polymer matrix, a robust hybrid organic-inorganic coating with further improved charge propagation capabilities has been formed. In this respect, the well-defined structure, excellent physicochemical stability, as well as the reversible multi-electron electrochemical reactions of Keggin-type polyoxometalates [15, 23–25] has been explored to produce novel functional materials for electrodes for the energy storage applications. PEDOT structures can be generated through oxidative polymerization of its monomer, 3,4-ethylendioxythiophene (EDOT), in aqueous solutions [15, 26]. Among important features is that, in presence of heteropolymolybdates, solubility of EDOT is increased and electropolymerization becomes feasible in aqueous medium. In general, polyoxometalates exist as metal-oxygen clusters of early transition metals, such as Mo (VI), W (VI), or V (V), typically in their high oxidation states [27]. Keggin-type heteropolyanions are probably the most common because of their easy preparation, strong acidity, and general (also thermal) stability [28, 29]. Their widespread applications in catalysis, medicine, as well as useful electronic and magnetic materials [23, 28, 30, 31] should also be mentioned. Functionalized polyoxometalated-based systems are often fabricated as hybrid organic-inorganic materials [32]. Then polyoxometalates can exist as building blocks linked with certain organic molecules or metal-organic complexes as bridging groups [33, 34].

In the present work, the concept of assembling copper phosphomolybdate within the organic (conducting polymer) coating (PEDOT/PyBA) is pursued. An ultimate goal has been to produce a dense stable film in which concentration of electrochemically active polyoxometalate redox centers is high. It can be expected that, by introducing copper (II) ions into the PEDOT/PyBA matrix, the void spaces between the polymer granular-type structures should decrease due to the possible attractive electrostatic and coordinating interactions of Cu (II) ions with carboxylate groups of PyBA and molybdate heteropolyanions. These features should lead to the formation of denser and more stable hybrid organic-inorganic coatings. Furthermore, the results of diagnostic electrochemical experiments are consistent with reversible electrochemical charging of the hybrid film during the repetitive reductions and oxidations. On the whole, the propagation of charge (electrons, protons) seems to be fast enough to make the proposed system potentially useful for electrochemical charge accumulation applications.

Experimental

Chemicals and materials

All chemicals used were of analytical grade purity. The electropolymerization of PEDOT/PyBA was performed in an aqueous medium consisting of 0.068 mol dm^{-3} 3,4-ethylenedioxythiophene, EDOT (Aldrich), 10 mg of 4--(pyrrole-1-yl) benzoic/PyBA (Aldrich) in 1 dm^{-3} of water. Heteropolyacid, $H_3PMo_{12}O_{40}$, PMo_{12}, was obtained from Fluka. Solutions were prepared using doubly distilled and subsequently deionized (Millipore Milli–Q) water. Experiments were carried out at room temperature. Electrochemical measurements were performed using CH Instruments (Model CHI 660) workstation (Austin, TX, USA). A glassy carbon disk (with a geometric area of 0.2 cm^2) was supplied by Mineral (Warsaw, Poland). The experiments (voltammetric potential cycling) were performed in a conventional three electrode system, where platinum wire served as a counter electrode, whereas the Ag/AgCl electrode was the reference electrode. Prior to each experiment, glassy carbon electrode was activated by polishing it with aqueous alumina slurries (with a grain size of 0.05 mm) on polishing cloth and then rinsed with distilled water. Unless indicated otherwise, $Cu_xH_yPMo_{12}O_{40}$-containing PEDOT/PyBA (PEDOT/PyBA-$Cu_xH_yPMo_{12}O_{40}$), coatings were produced on glassy carbon by voltammetric cycling from −0.4 to 1.2 V for 3000 s at 50 mV s^{-1} in the modification solution containing 30 mmol dm^{-3} Cu_xH_y $PMo_{12}O_{40}$ and 0.068 mol dm^{-3} EDOT (together with 10 mg of PyBA in 1 dm^{-3} water). The solution of 0.5 mol dm^{-3} H_2SO_4 was used as proton conducting supporting electrolyte. The electrode materials were assembled as disks (geometric area, 0.2 cm^2) into the capacitor-type half cells placed within Swagelok holders. They were tested using the charging-discharging galvanostatic (CH Instruments Model CHI 760E) analyzer operating in the potential range from −0.2 to 0.5 V.

A porous glassy fibrous paper (Aldrich), that had been presoaked in the H_2SO_4 electrolyte, was used as a separator. Electrodes were assembled parallel in the two electrode

sandwich-type configuration. All measurements were executed following 24 h from the time of assembling. Mass of the electrode materials was about 0.0011 g (±2 mg).

Characterization techniques

The coating thicknesses were determined using (Talysurf 50, Rank Taylor Hobson) profilometer. The thickness of the PEDOT/PyBA-$Cu_xH_yPMo_{12}O_{40}$ coating (deposited on glassy carbon) was found to be equal to ca. 0.60 μm. Scanning electron microscopy (SEM) images were obtained using JOEL (Model 6610LV) instrument. Infrared spectra were measured with Shimadzu 8400 Fourier transform infrared (FTIR) spectrometer. The coating adhesion tests were performed with use of scratch tape. Before the adhesion test, the respective modified electrode was rinsed with distilled water and dried at ambient conditions. Later, the scotch tape was sticked to the surface. The tape was detached rapidly. The amount of modified material on the scotch tape indicated the adhesivity of the surface coating. It is noteworthy that only after 20 scotch tape-detaching tests, the beginning of decohesion of the PEDOT/PyBA-$Cu_xH_yPMo_{12}O_{40}$ coating became visible. This adhesion test allows to conclude about the reasonably strong attachment of the coating to the electrode substrate.

Surface elemental analysis was performed with X-ray photoelectron spectroscopy (XPS) Microlab 350 Thermo VG Scientific) instrument. XPS measurements were carried out using AlKa radiation (10 kV; 10 mA). Depth profiles were obtained via Ar^+ sputtering at 5 kV (ion gun emission current in the range of 1–10 mA). The XPS spectra were analyzed using the NIST XPS database [35, 36].

Preparation of copper heteropolymolybdate salt

The $H_3PMo_{12}O_{40}$ (PMo_{12}) heteropolyacid was prepared as described earlier [37]. The first involved preparation of the barium salt by ionic exchange of the acidic protons by barium cations. The copper salts of the Keggin-type $PMo_{12}O_{40}^{3-}$ were subsequently obtained by a successive ionic exchange between barium and copper cations. The respective reactions are as follows:

$$\left(3H^+, \cdot PMo_{12}O_{40}^{3-}\right)\cdot + \cdot\left(1.5Ba^{2+}, \cdot 3OH^-\right)\cdot \rightarrow \cdot\left(1.5Ba^{2+}, \cdot PMo_{12}O_{40}^{3-}\right)\cdot + \cdot 3H_2O \quad (1)$$

$$\left(1.5Ba^{2+}, \cdot PMo_{12}O_{40}^{3-}\right)\cdot + \cdot\left(1.5Cu^{2+}\cdot + \cdot SO_4^{2-}\right)\cdot \rightarrow \cdot\left(1.5Cu^{2+}, \cdot PMo_{12}O_{40}^{3-}\right)\cdot + \cdot BaSO_4^{2-} \quad (2)$$

The reactants were introduced at stoichiometric quantities and stirred vigorously at room temperature. The solution of the copper salt was then filtered to eliminate the $BaSO_4$ white precipitate. Then the remaining solution was evaporated at room temperature to obtain $Cu_xH_yPMo_{12}O_{40}$ solid.

In order to verify the chemical composition of the $Cu_xH_yPMo_{12}$ salt, an XPS analysis was performed in a wide binding energy range (Fig.1a). On its basis, the following elements can be identified: Mo, O, Cu, P, Al, C, and Mg. The peaks for Al, Ci Mg, as possibly from the aluminum foil, were omitted in the quantitative analysis. But Mo, Cu, and P are constituents of the powder. Ascribing the Mo, O, Cu, and P peaks to the powder, the elementary composition of the examined powder was determined upon considering areas under the peaks (Table 1). The results are consistent with the following salt's approximate stoichiometry: $CuHPMo_{12}O_{40}$ (rather than $Cu_{1.5}PMo_{12}O_{40}$). Because the relative amounts of Cu and Mo may change during utilization of the system under electrochemical conditions, the $Cu_xH_yPMo_{12}O_{40}$ notation is proposed and used throughout the text here.

Predominant elements in the material under investigation are molybdenum and oxygen. Copper and phosphorous appear at relatively lower amounts. Nevertheless, the presence of copper is clearly apparent from the spectrum within the binding energy region characteristic of copper (II), as shown in Fig. 1b. Indeed, the peak referring to copper, especially the $2p_{3/2}$ peak, can easily be distinguished here. Copper is characterized by a relatively low XPS detection coefficient, namely atomic sensitivity factor (ASF) on the level 4.3. Here, identification of copper in the atomic concentration of merely ~0.004 has been possible.

Results and discussion

Fabrication of PEDOT/PyBA-$Cu_xH_yPMo_{12}O_{40}$ coating

Controlled electrodeposition of hybrid coatings of PEDOT/PyBA together with the Keggin-type salt of $Cu_xH_yPMo_{12}O_{40}$ was achieved by voltammetric potential cycling as described in Experimental section.

Among comparative measurements, first, electrodeposition of PEDOT coating on glassy carbon (Fig. 2a) has been considered here. In the first cycle, an increase in current density is observed in the potential range above 0.9 V which suggests formation of PEDOT in the oxidized form [26]. During the return potential scan, a negative current peak appears at ca. −0.1 V which shall be associated with the reduction of the oxidized polymer layer deposited on the electrode. During subsequent polarization cycles, the oxidation and reduction peaks are becoming higher which is indicative of the PEDOT coating buildup. However, over the course of time, the coating buildup process is gradually inhibited. Indeed, one

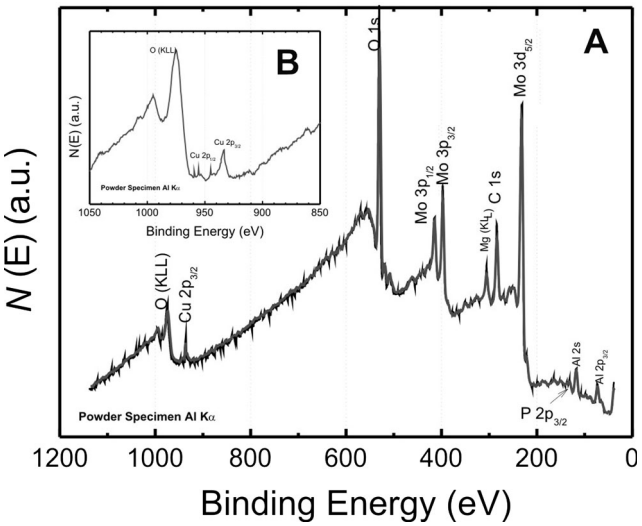

Fig. 1 XPS spectrum of the $Cu_xH_yPMo_{12}O_{40}$ material deposited onto aluminum foil (**a**). The XPS spectrum of $Cu_xH_yPMo_{12}O_{40}$ is recorded in a narrow binding energy range (appropriate for identification of Cu) (**b**)

can observe changes in shapes of peaks in addition to decreasing differences in magnitudes of the current densities recorded during in successive potential cycles. It was postulated [38] that the PEDOT coating growth slowdown was caused by the slow diffusion of the monomer from the solution. A similar phenomenon has been observed here for the PEDOT/PyBA coating, as shown in Fig. 2b. In a case of such a functionalized organic conducting polymer as PEDOT/PyBA, some of the positively charged PEDOT sites may interact electrostatically with the anion carboxyl groups (originating from PyBA).

Figure 2c illustrates the growth of the hybrid PEDOT/PyBA-$Cu_xH_yPMo_{12}O_{40}$ coating, as evidenced from the increase of the peak currents during the first 47 voltammetric cycles. Due to the possibility of structural reorganization of $Cu_xH_yPMo_{12}O_{40}$ (hydrogen evolution), the negative potential scan excursions have been limited to −0.4 V. The result is consistent with the view that the PEDOT organic polymer coatings (Fig. 2a) have been generated on the electrode surface during positive potential scans [39–42] whereas PyBA and $Cu_xH_yPMo_{12}O_{40}$ nanostructures have been simultaneously attracted during potential cycling and growth of the coatings.

During electrodeposition of a PEDOT/PyBA-$Cu_xH_yPMo_{12}O_{40}$, in each cycle, we have observed gradual increases of current densities related to respective oxidations and reductions (see peaks in Fig. 2c). The phenomenon is consistent with the fairly uniform distribution of the phosphomolybdate polyanion within the growing hybrid organic-inorganiuc film.

Table 1 The surface atomic concentration of the test material in powder form

Element	Mo	Cu	P	O
Atomic concentration	0.259	0.022	0.021	0.698

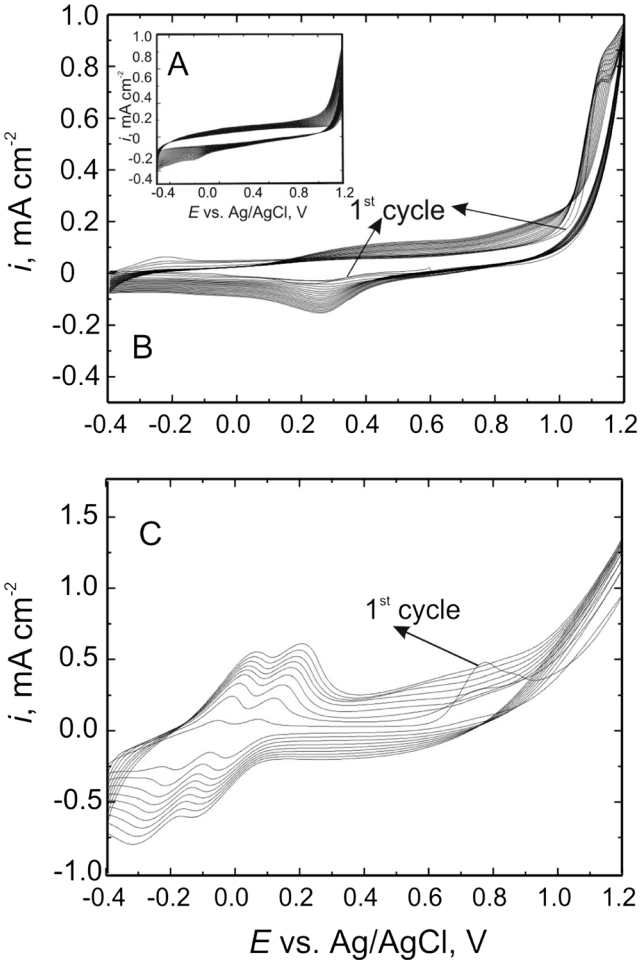

Fig. 2 Voltammetric generation (electrodeposition) of **a** PEDOT, **b** PEDOT/PyBA, and **c** PEDOT/PyBA-$Cu_xH_yPMo_{12}O_{40}$ coatings from the appropriate solutions for modification. Scan rate, 0.05 mV s^{-1}

Physicochemical properties of PEDOT/PyBA-$Cu_xH_yPMo_{12}O_{40}$

Regardless of the fact that the hybrid coating contained both the fast electron transfer (Keggin-type phoshomolybdates) and the electronically conducting (PEDOT) components, attention has been paid to the systems' morphology, porosity, and chemical identity. Obviously, the latter features affect the materials ability to propagate charge (ions, electrons) during redox transitions.

The results of SEM measurements performed for the PEDOT, PEDOT/PyBA, and PEDOT/PyBA-$Cu_xH_yPMo_{12}O_{40}$ coatings are illustrated in Fig. 3a, d. In all cases, the surface structure is granular. The PEDOT polymer coating itself is very compact and made up of closely adjacent grains with diameters of approx. 200–300 nm. Similar morphologies were observed before [43] during monitoring electropolymerization of PEDOT in organic solvents. The grain sizes of the simple PEDOT film are smaller when compared to sizes of grain agglomerates of PEDOT/PyBA. It is likely that, in the presence of PyBA, the growth of PEDOT

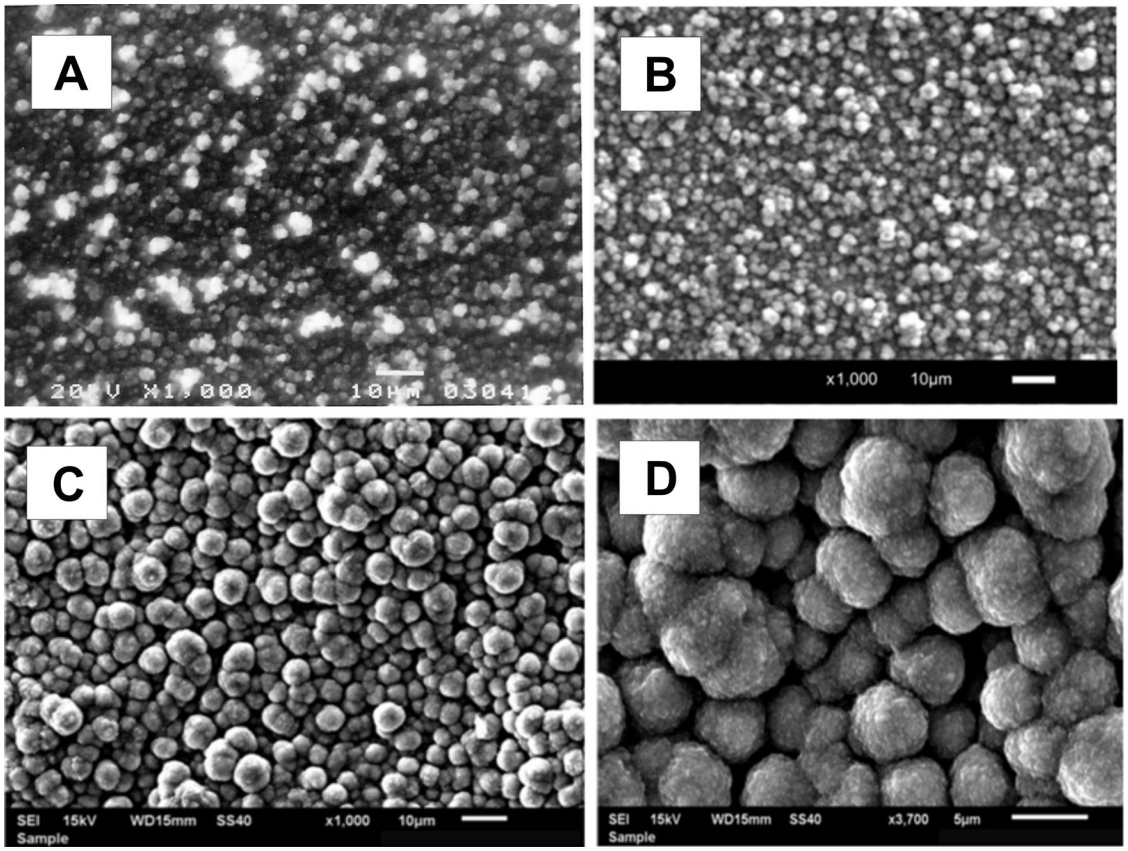

Fig. 3 SEM images of **a** PEDOT, **b** PEDOT/PyBA, and c PEDOT/PyBA-$Cu_xH_yPMo_{12}O_{40}$ coatings on glassy carbon

has been somewhat induced by hydrophilic carboxyl groups. During the growth of the hybrid film, both heteropolymolybdate anions (from the $Cu_xHyPMo_{12}O_{40}$ salt) and carboxyl groups (from PyBA) may interact with the positively charged PEDOT backbone (in the oxidized state). Furthermore, the copper (II) ions (from the $Cu_xHyPMo_{12}O_{40}$ salt) should be attracted and stabilized by PyBA carboxyl groups. Examination and comparison of the respective SEM images allow one to conclude that the PEDOT/PyBA-$Cu_xH_yPMo_{12}O_{40}$ coating is more porous in relative to other coatings studied here.

On mechanistic grounds, it is reasonable to expect that, at the first stage, a uniform coating has been most likely deposited on the surface. This step has been followed by formation of grains that tended to grow. The formation of grains on the surface and their subsequent expansion from Fig. 3c, d (SEM data) and from Fig. 4 (AFM data), the grains have diameters ranging from several 100 nm to 1 μm. In a case of the hybrid film, the grains seem to be more uniformly distributed on the electrode surface. The fact that the layer is still porous permits the electrolyte ions to penetrate the hybrid film.

Figure 5 presents the infrared spectrum of heteropolyacid. The observed peaks have been verified using literature data [15, 37, 44–48]. The main features typical for the Keggin phosphomolybdate structure have been observed for both $H_3PMo_{12}O_{40}$ and $Cu_xH_yPMo_{12}O_{40}$ systems. The band frequencies (in cm^{-1}) characteristic of $H_3PMo_{12}O_{40}$ and $Cu_xH_yPMo_{12}O_{40}$ have been as follows: 760 to 748, 875 to 845, 972 to 961, and 1075 to 1060 cm^{-1}; and they shall be assigned to bands characteristic of Mo–O (edge sh) –Mo, Mo–O (corner sh) –Mo, Mo=O (terminal), and P–O (oxygen bridging P heteropolyatom) stretching vibrations. The band around 1610 to 1590 cm^{-1} (appearing in both $H_3PMo_{12}O_{40}$ and $Cu_xH_yPMo_{12}O_{40}$) is due to the presence of oxonium ions (H_3O^+) and/or "neutral" water.

The FTIR spectra of PEDOT, PyBA, and PEDOT/PyBA were reported before [47]. Figure 6 shows the FITR spectrum of PEDOT/PyBA-$Cu_xH_yPMo_{12}O_{40}$ coating deposited on glassy carbon. The spectrum of $Cu_xH_yPMo_{12}O_{40}$ is also provided. When compared to Fig. 4, the frequencies of characteristic vibrations for the $Cu_xH_yPMo_{12}O_{40}$ heteropolyacid salt are shifted from value to value: 1060 to 1093, 961 to 951, 845 to 884, and 748 to 755 cm^{-1}.

The spectrum of the PEDOT/PyBA-$Cu_xH_yPMo_{12}O_{40}$ coating cannot be regarded as a simple superposition of the PEDOT, PyBA, and $Cu_xH_yPMo_{12}$ spectra. For example, the characteristic bands of PEDOT are not only shifted, but also significantly altered upon incorporation of PyBA. On the other hand, a characteristic peak observed The PyBA peak at 2137 cm^{-1} should also be noted here. The PyBA had

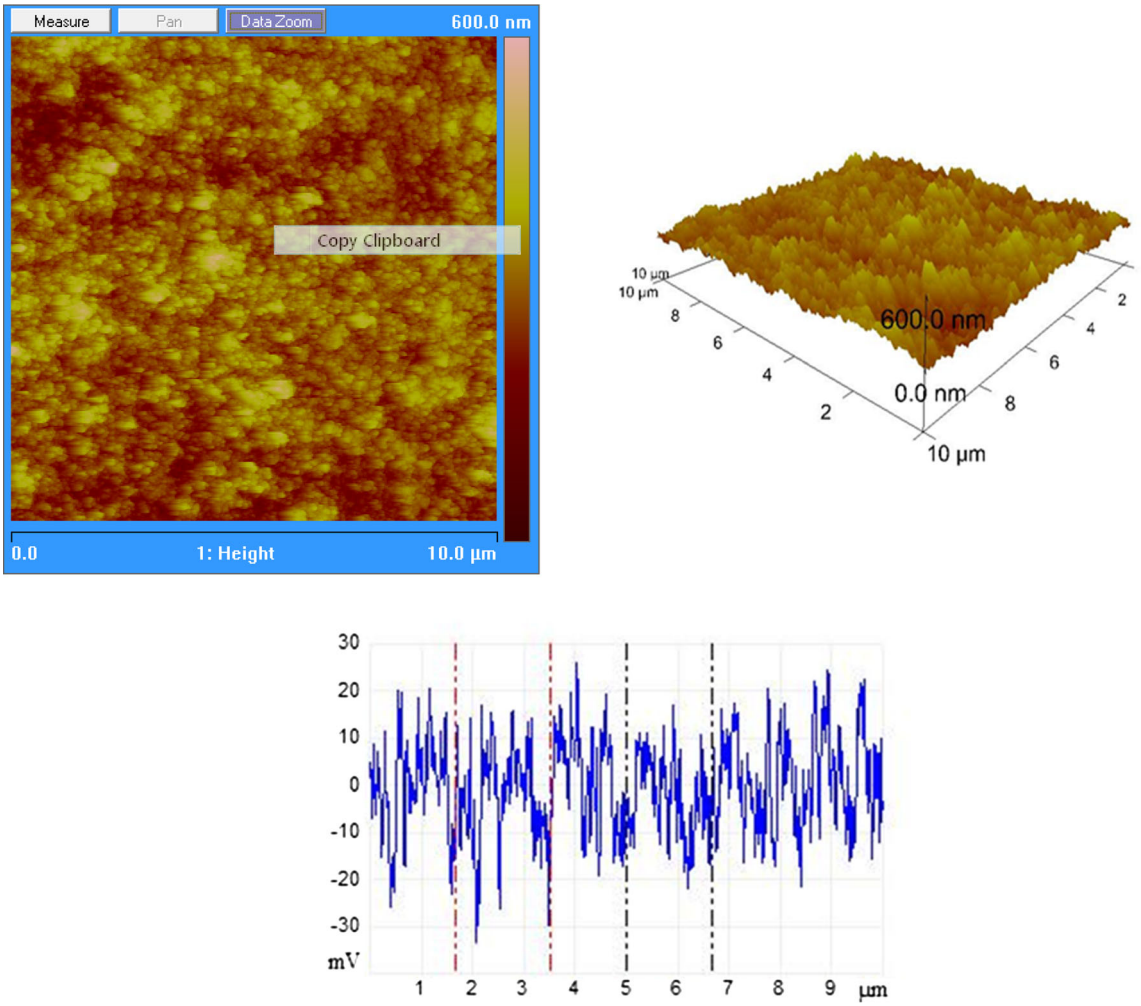

Fig. 4 AFM topography of the PEDOT/PyBA-$Cu_xH_yPMo_{12}O_{40}$ coating in the three-dimensional projection with a depth profile (using SiN probe)

undergone some polymerization (around the pyrrole ring) after voltammetric potential cycling. The peaks that are observed from 1053 to1208 cm^{-1} have most likely originated from the stretching in the alkylenedioxy group. The system (Fig. 6) is characterized by two well-defined peaks in the range of frequencies from 1400 to 1600 cm^{-1}, being typically attributed to the pyrrole ring stretching modes [49]; but the –CO stretching mode of the carboxylic group has been observed at 1640 cm^{-1} in the spectrum. This frequency is characteristic of the undissociated group. Interestingly, the absorption peak at 1640 cm^{-1} has been associated with the doping level of PEDOT. Chevrot and co-workers assigned the peak at 1640 cm^{-1} to the C=C bond, whose position depended on the doping level of the polymer [50].

Electrochemical properties of PEDOT/PyBA-$Cu_xH_yPMo_{12}O_{40}$

Figure 7(a) shows the cyclic voltammetric response recorded after electrodeposition of the PEDOT/PyBA-$Cu_xH_yPMo_{12}O_{40}$ coating in a 0.5 mol dm^{-3} H_2SO_4 solution. The coatings in Figs 7(a–c) have been deposited using the same parameters (scan rate of 0.5 mV s^{-1}; deposition time of 3000 s; and the potential interval from −0.4 to 1.2 V). Because the Keggin-type heteropolyanions are unstable in both neutral and basic media, an acid medium has been chosen here. To avoid interferences from the hydrogen evolution reaction at negative potentials and the irreversible copper phosphomolybdate reduction reactions at potentials lower than −0.2 V (lower potential values cause the reorganization of the system structure), the discussion has been limited here to three pairs of voltammetric peaks. For comparison, the voltammogram for the PEDOT/PyBA coating is shown in Fig. 7(c)). No distinct anodic or cathodic peaks (oxidation and reduction peaks) for PEDOT/PyBA have observed here. Literature reports reveal that, in aqueous solutions, the oxidation and reduction overlapping processes existed in the potential interval from −0.2 to 0.8 V [15] and the capacitive-type behavior was postulated then. By contrast, the

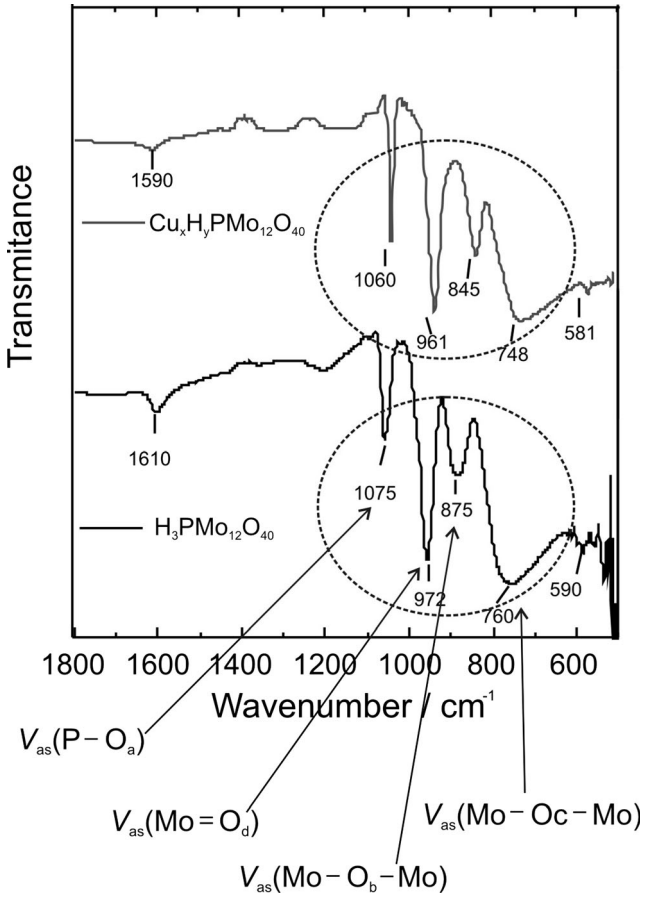

Fig. 5 FTIR spectra of a $H_3PMo_{12}O_{40}$ and $Cu_xH_yPMo_{12}O_{40}$ in KBr. Symbols used O_a—oxygen bridging P heteropolyatom, O_b—corner sharing oxygen, O_c—edge sharing oxygen belonging to the WO_6 octahedra, and O_d—terminal oxygen

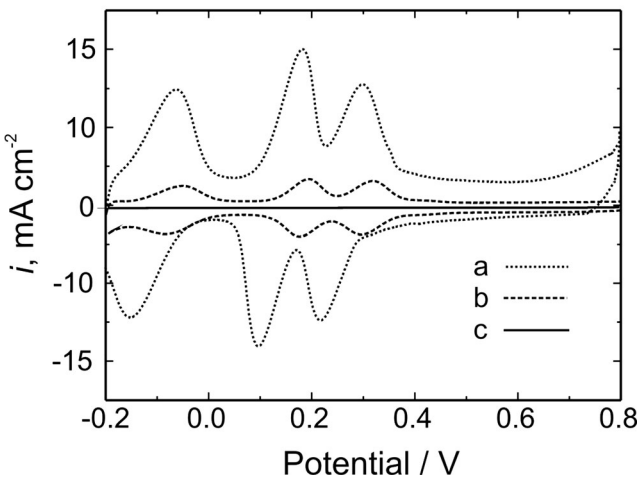

Fig. 7 Cyclic voltammetric responses of *a* PEDOT/PyBA-$Cu_xH_yPMo_{12}O_{40}$, *b* PEDOT/PyBA-$H_3PMo_{12}O_{40}$, and *c* PEDOT/PyBA coatings on glassy carbon. Electrolyte 0.5 mol dm^{-3} H_2SO_4. Scan rate, 50 mVs^{-1}

voltammograms shown in Fig. 7(a, b) have three pairs of well defined and reversible peaks originating from the electroactivity of heteropolyacid. The current densities of the cathodic and anodic peaks for the PEDOT/PyBA/$Cu_xH_yPMo_{12}O_{40}$ coating are much higher (thus implying incorporation of larger populations of polymolybdates), and they are somewhat shifted toward negative potential values, when compared to PEDOT/PyBA-$PMo_{12}O_{40}$ coating. According to the literature data [15, 51–53], the redox reactions of the PMo_{12} are interpreted in terms of three consecutive two electron processes and can be described as follows:

$$PMo_{12}O_{40}^{3-} + ne^- + nH^+ \rightleftarrows H_nPMo_{12}O_{40}^{3-} \quad (3)$$

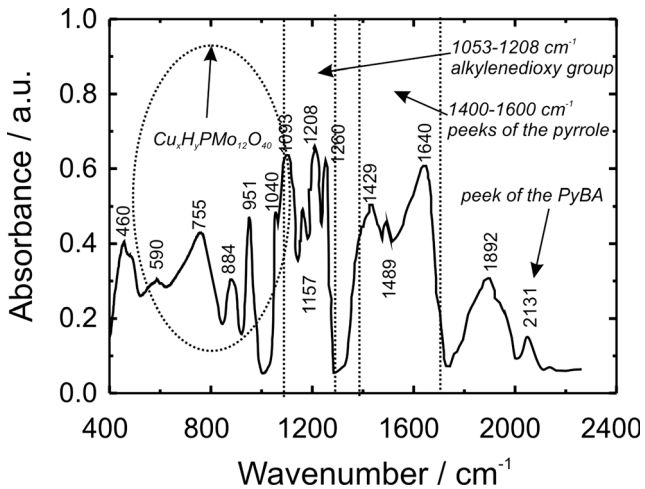

Fig. 6 FTIR spectrum of the optimum PEDOT/PyBA-$Cu_xH_yPMo_{12}O_{40}$ coating deposited on glassy carbon

Figure 8 illustrates voltammetric responses of the PEDOT/PyBA-$Cu_xH_yPMo_{12}O_{40}$ coating (deposited as for Fig. 2c), recorded upon application of different potential scan rates. The plot of the dependence of cathodic peak currents (measured at 0.16 V on scan rate yields nearly linear relationship (effectively, with a zero intercept) up to the scan rate value of 0.1 V s^{-1}. Under such conditions, the latter behavior is consistent with the surface-type behavior of the system. Such a relationship also implies the fast dynamics of charge transfer in the vertical direction, i.e., perpendicularly to the electrode direction.

There is also an indirect evidence for the presence of copper in the investigated layers (Figs. 7 and 8). Upon careful examination of voltammetric responses of the $Cu_xH_yPMo_{12}O_{40}$-containing systems, one can find that both anodic (at ca. 0.2 V) and cathodic (at −0.17 V) peaks are somewhat 15–20 % higher than the respective counter cathodic (at 0.08 V) and anodic (at −0.05 V) peaks. Such differences have not been observed in the voltammetric responses of the Cu-free polymolybdate containing materials. Apparently, there is a mutual overlapping of redox processes of PMo_{12} and Cu/Cu^{+2} redox couple. The fact that copper peaks are largely hidden is consistent with the relatively lower than

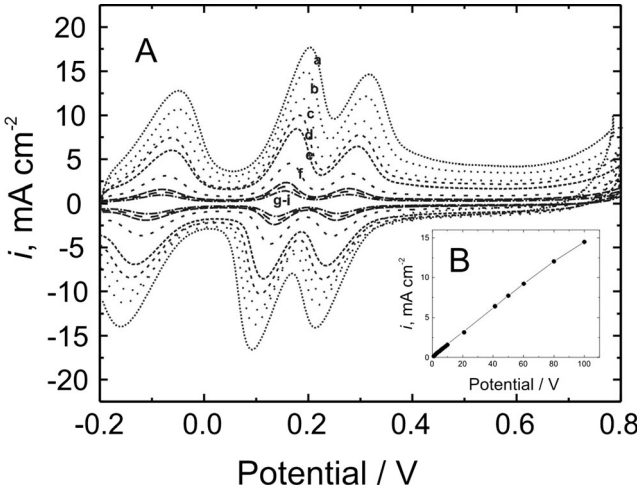

Fig. 8 **a** Cyclic voltammetric responses of the optimum PEDOT/PyBA-$Cu_xH_yPMo_{12}O_{40}$ coating recorded at different scan rates: *a* 100, *b* 50, *c* 40, *d* 30, *e* 20, *f* 8, *g* 5, *h* 2.5, and *i* 1 mV s^{-1}. **b** *Inset*: dependence of the reduction peak current (measured at 0.2 V) on scan rate. Other conditions as for Fig. 6

stoichiometric concentration of copper in the salt. The presence of copper has been evident from EDX (coupled to SEM) analytical data. We are unable to provide the precise value, but we expect copper to be present on the level of 20 % of its initial value ($CuHPMo_{12}O_{40}$). It is reasonable to expect that positively charged units of PEDOT (in the conducting state) replace positions of copper cations and provide the overall electro neutrality in the hybrid films. The indirect proof for the presence of copper in the system is its increased stability during potential cycling (50 mV s^{-1}) for 20 h in the potential range under conditions of Fig.8. Indeed, there has not been practically any decrease in the system's characteristic peak currents. On the other hand, the analogous experiments utilizing the Cu-free hybrid film have resulted in almost 40 % decreases.

Another important issue of the data of Fig. 8 (inset) is that the voltammetric peak currents are proportional to the scan rate up to 100 mV s^{-1}. This linear dependence clearly implies the system's ability to propagate charge fast enough to assure effectively the surface-type characteristic regardless the fact the coating of ca. 0.6 μm thickness largely exceeds the monolayer-type coverage. Apparently, the mixed valence Mo (VI V) sites are effectively at sufficiently large population to make the fast electron transfers feasible. Furthermore, the presence of the conducting polymer matrix contributes to the overall fast charge distribution. High porosity of the material (SEM and AFM data) is in this respect also advantageous.

Galvanostatic charging/discharging

Judging from the electrochemical characteristics described above, the electrode material presented here does not yield quasi rectangular cyclic voltammograms but, instead, it demonstrates pure Faradic behavior, namely redox reactions, which have nothing to do with capacitance. In other words, the performance of the PEDOT/PyBA-$Cu_xH_yPMo_{12}O_{40}$ system is analogous to that of the thin laye "battery" type material. Therefore, instead of determining capacitance (in F/g), that is applicable to the "supercapacitive"-type systems, the capacity (in C/g) should be considered here [1, 2].

The values of capacities are obviously dependent on a method of their determination. For example, a two electrode cell represents a real charge storage device, but it does not permit controlling performance of single electrodes in the total charge accumulation. The simplest, but useful, preliminary approach is based on voltammetry performed at scan rates as low as 1 to 5 mV s^{-1}. The average capacitive current estimated from the current-potential dependence allows also estimation of the optimal current for galvanostatic charging/discharging experiments. Here, in a case of the hybrid system composed of the conducting polymer/polyoxometalate salt (characterized by largely developed microporous surface area), the capacity equal to 38.5 C g^{-1} has been determined from cyclic voltammetry method using the following parameters: potential interval, −0.2 to 0.8; scan rate, 20 mV s^{-1}; electrode mass, 0.011 g; electrolyte 0.5 mol dm^{-3} H_2SO_4.

The materials have also been subjected to galvanostatic cycling upon application of current densities ranging from 0.042 to 0.33 A g^{-1}; and the dependencies of potential (*U*) on time have been measured (Fig. 9). The observed charging-discharging profiles are reversible and reproducible. They have also largely linear portions which may implies performance characteristic of the low resistance battery. In this respect, the increased materials hydrophilicity (due to the presence of PyBA [17] and structurally hydrated Keggin-type polyoxometalate [10–13]) is of importance here.

It is noteworthy that the battery-type cell utilizing the hybrid organic-inorganic PEDOT/PyBA-$Cu_xH_yPMo_{12}O_{40}$ system has exhibited a sustained cycle ability over the fairly long period of time of cycling. Figure 10 illustrates the dependence

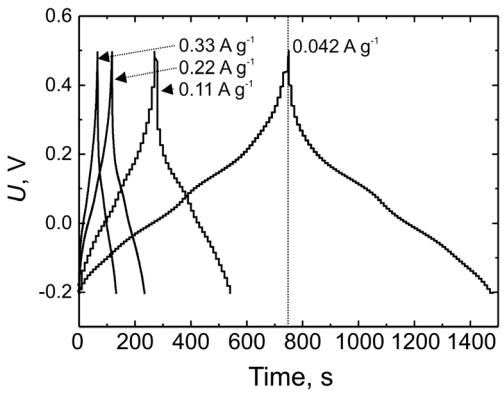

Fig. 9 Galvanostatic charging/discharging patterns for the battery-type two-electrode cell utilizing PEDOT/PyBA-$Cu_{1.5}PMo_{12}O_{40}$ recorded upon application of currents ranging from 0.042 to 0.33 A g^{-1}

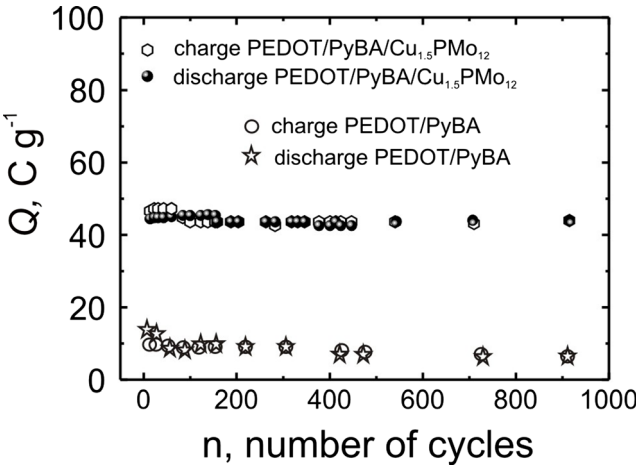

Fig. 10 Dependencies of capacities on the number of charging-discharging cycles plotted for PEDOT/PyBA-$Cu_xH_yPMo_{12}O_{40}$ and PEDOT/PyBA. Current density, 0.042 A g^{-1}; potential range −0.2–0.5 V. Other conditions as for Fig.9

of capacity over as many as 900 cycles. It should be noted that this dependence has been plotted following diagnostic experiments performed at different current densities as for Fig. 9. The overall good long-term cycle stabilities of PEDOT/PyBA-$Cu_xH_yPMo_{12}O_{40}$ and PEDOT/PyBA in 0.5 mol dm^{-3} H_2SO_4 electrolyte have been assessed on the basis of the numerous galvanostatic charging-discharging tests performed between −0.2 and 0.5 V at the current density of 0.042 A g^{-1} (900 cycles, as shown in Fig. 10). For simplicity, in the present work, the performance of copper-free system of PEDOT/PyBA and phosphomolybdate is not considered because of its insufficient stability (PMo_{12}-leaching) over the period cycling (900) explored here. It is apparent from Fig. 9 that only a small decrease in capacity occurs during initial cycling and, later, the capacity tends to stabilize. After 900 cycles, the capacity values have decreased only by 10 % from the original value. It can be concluded that PEDOT/PyBA-$Cu_xH_yPMo_{12}O_{40}$ battery-type material exhibits reasonable cycle stability (Fig. 9) and a high degree of reversibility (Fig. 10) in acid electrolyte during repetitive charging-discharging. The capacity values characteristic of the charge storage devices built of PEDOT/PyBA-$Cu_xH_yPMo_{12}O_{40}$ and PEDOT/PyBA, as calculated from the charging-discharging curves (upon application of 0.042 A g^{-1}) were 41.3 and 12.6 C g^{-1} (Fig. 10). These results are a few percent higher than those estimated from conventional voltammetric curves.

Remembering that charging-discharging profiles, the optimum PEDOT/PyBA-$Cu_xH_yPMo_{12}O_{40}$ system (Fig. 9) is quasi symmetric (the same comment applies to PEDOT/PyBA, but for simplicity the respective data are not shown here). Consequently, the following parameters can be estimated from the galvanostatic charging-discharging curves using the following relation:

$$Q_m = i\frac{t}{m} \tag{4}$$

where Q_m is the experimental capacity per mass unit, i is the constant charging-discharging current, t discharging time, and m is the mass of the electrodes material. Furthermore, the specific capacity (per gram), Q_{spec}, has been calculated (from discharging segments; Fig. 11a):

$$Q_{spec} = \frac{2it}{m} \tag{5}$$

Figures 11 and 12 illustrate dependencies of capacities (Q_m and Q_{spec}) of the optimum PEDOT/PyBA-$Cu_xH_yPMo_{12}O_{40}$ and the simple PEDOT/PyBA that have been determined in two ranges of charging-discharging current densities: low from 20 to 220 mA g^{-1} (Figs. 11b and 12b) and relatively higher from 20 to 870 mA g^{-1} (Figs. 11a and 12a). The maximum value of the cell capacity equal to 42.7 C g^{-1} has been achieved at the current density of 20 mA g^{-1} (Fig. 11a). For current density values higher than 220 mA g^{-1}, a rapid decrease in capacities has been observed down to 5.6 C g^{-1}. In the present work, the effect of high current densities on the

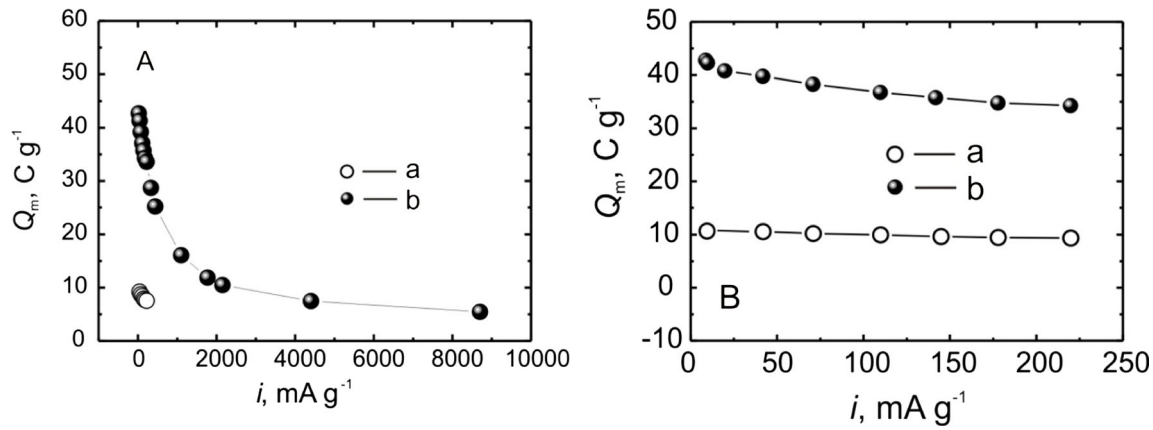

Fig. 11 Dependencies of capacity on increasing discharging currents plotted for *a* PEDOT/PyBA and *b* PEDOT/PyBA-$Cu_xH_yPMo_{12}O_{40}$ in two distinct ranges of currents: **a** from 0.02 to 8.7 A g^{-1} and **b** below 220 mA g^{-1}

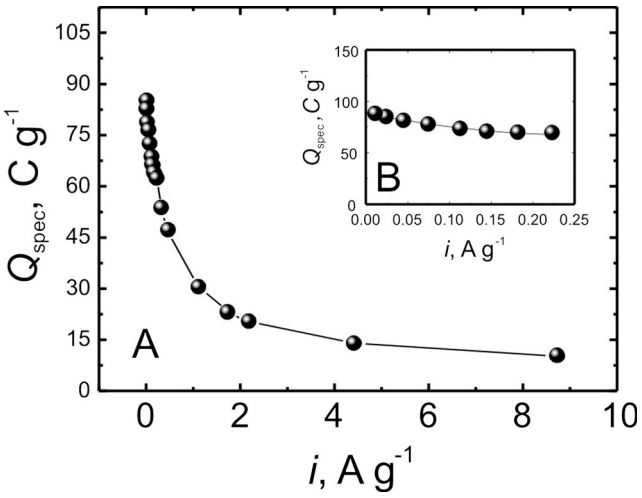

Fig. 12 Dependecies of specific capacity on increasing discharging currents plotted for the optimum PEDOT/PyBA-$Cu_xH_yPMo_{12}O_{40}$ system in two distinct ranges of currents: **a** from 0.02 to 8.7 A g^{-1} and **b** below 220 mA g^{-1}

systems' capacity and power parameters has been intentionally addressed. An important feature of the optimum PEDOT/PyBA-$Cu_xH_yPMo_{12}O_{40}$ system is that the increase in current density from 8 to 220 mA g^{-1} has resulted in only in moderate decreases (Figs. 11b and 12b) in capacitances (Q_m and Q_{spec}) from 42.7 to 35 C g^{-1} and from 85.4 to 70 C g^{-1}. In other words, the performance of PEDOT/PyBA-$Cu_xH_yPMo_{12}O_{40}$ is consistent with the reasonably good durability of capacity in the current density range up to 220 mA g^{-1}. In this respect, electronic conductivity of PEDOT and rates of charge (electron, proton) transport are high enough to assure unimpeded charge distribution. At higher discharging, currents various limitations start to appear. In addition to possible kinetic limitations, it should be remembered that the PEDOT/PyBA-$Cu_xH_yPMo_{12}O_{40}$ film is not an ideal surface-type system. The enforced current flow, both under discharging conditions of Figs. 11 and 12 and in cyclic voltammetry (Fig. 8) at high scan rates, e.g., >>100 mV s^{-1}, where linear dependence on scan rate (inset to Fig. 8) and the surface-type behavior are not be applicable anymore, would also lead to the development of less effective" diffusional-type concentration gradients regardless the actual charge propagation mechanisms.

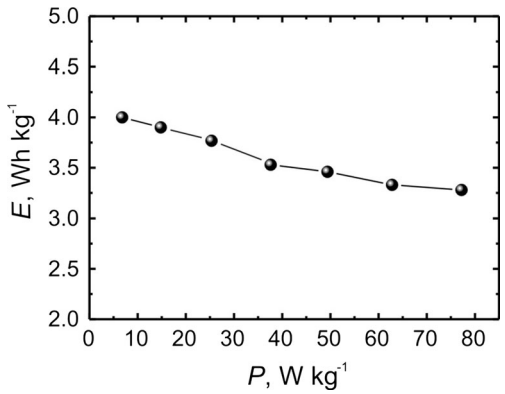

Fig. 13 Dependency of the specific energy density on the specific power (Ragone plots) prepared using the charging/discharging data for the optimum PEDOT/PyBA-$Cu_xH_yPMo_{12}O_{40}$ system

Using the galvanostatic data of Figs. 11b and 9, such parameters as the energy and power densities have been determined for the optimum PEDOT/PyBA-$Cu_xH_yPMo_{12}O_{40}$ system (utilized within the two-electrode battery-type cell) and correlated in a form of so-called Ragone plot. Figure 13 shows the respective dependence of the energy density as a function of the power density. Here, the maximum energy density value was equal to 4 Wh kg^{-1} at the power density of 6.8 W kg^{-1} and the discharging current of 20 mA g^{-1}. Successful utilization of higher charging/discharging currents would require optimization of the materials morphology and composition as well as addition of such carbon nanostructures as nanoparticles (blacks) or nanotubes to further improve distribution of charge.

Conclusions

This work discusses utility of a new type the hybrid organic-inorganic system composed of PEDOT/PyBA and $Cu_xH_yPMo_{12}O_{40}$ three-dimensionally distributed within ca 0.6 μm films on the glassy carbon electrode surfaces. The attractiveness of the composite system concerns the fact that formal potentials of the Cu_xHyPMo_{12} redox processes lie in the potential range where PEDOT is conductive. Morphology of the hybrid coating is fairly dense, but the system is still porous. The formation of the hybrid PEDOT/PyBA-$Cu_xH_yPMo_{12}O_{40}$ materials was confirmed by FTIR, XRD, AFM, SEM, and electrochemical methods. Good stability of the hybrid organic-inorganic coating may originate from the existence of attractive electrostatic and chemical interactions between positively charged PEDOT, carboxylic groups of PyBA, copper (II) cations, and phosphomolybdate (anionic) components. The hybrid materials have been examined (in addition to microscopic imaging) as the electrode material for charge storage application using both conventional voltammetric and galvanostatic approaches. Despite the fact that the proposed coatings are as thick as 0.6 μm, the materials exhibit reversible behavior characteristic for the fast surface-type systems on electrodes. Utilization of copper (II) results in the sound stabilization effect without losses in the overall dynamics of charge propagation. Although no attempt was made to optimize the construction of the charge storage device, the parameters obtained here (specific capacity, 80 C g-1; energy density, 4 Wh kg^{-1}, and the power density of 6.8 W kg^{-1}) make the system potentially attractive for the accumulation of charge with the use of electrodes modified with thin hybrid organic-inorganic systems. The results could get further

improved by optimization of the thickness, morphology, and through addition of largely dispersed carbon nanostructures (blacks, nanotubes, etc.). Further research is along this line.

Acknowledgments The author acknowledges financial support from the Ministry of Science and Higher Education (Poland) number project: BS/PB–207–301/09 and National Science Center, Grant No. NN 507 322040.

The author would also like to thank P.J. Kulesza for the helpful discussions regarding this manuscript.

References

1. Brousse T, Belanger D, Long JW (2015) To be or not to be pseudocapacitive? J Electrochem Soc 162(5):A5185–A5189
2. Simon P, Gogotsi Y, Dunn B (2014) Where do batteries end and supercapacitors begin? Mater Sci 343:1210–1211
3. Winter M, Brodd RJ (2004) What are batteries, fuel cells, and supercapacitors? Chem Rev 104:4245–4269
4. Ragoisha GA, Aniskevich YM (2016) False capacitance of supercapacitors. http://arxiv.org/abs1604.08154
5. Conway BE (1999) Electrochemical supercapacitors. Scientific fundamentals and technological applications. Kluwer Academic, Plenum Publishers
6. Kulesza PJ, Malik MA, Wieckowski A (eds) (1999) Interfacial electrochemistry− theory experiment and applications, solid–state voltammetry 673. Marcel Dekker, New York
7. Kulesza PJ, Cox JA (1998) Solid-state voltammetry—analytical prospects. Electroanalysis 73:10(2)73−80
8. Kulesza PJ, Dickinson E, Williams ME, Hendrickson SM, Malik MA, Miecznikowski K, Murray RW (2001) Electron self-exchange dynamics of hexacyanoferrate in redox polyether hybrid molten salts containing polyether-tailed counterions. J Phys Chem B 105: 5833–5838
9. Surridge NA, Jernigan JC, Dalton EF, Buck RP, Watanabe M, Zhang H, Pinkerton M, Wooster TT, Longmire ML, Facci JS, Murray RW (1989) The electrochemistry group medal lecture. Electron self-exchange dynamics between redox sites in polymers. Faraday Discuss Chem Soc 88:1–17
10. Kulesza PJ, Chojak M, Karnicka K, Miecznikowski K, Palys B, Lewera A, Wieckowski A (2004) Network films composed of conducting polymer-linked and polyoxometalate-stabilized platinum nanoparticles. Chem Mater 16:4128–4134
11. Kulesza PJ, Pieta IS, Rutkowska IA, Wadas A, Marks D, Klak K, Stobinski L, Cox JA (2013) Electrocatalytic oxidation of small organic molecules in acid medium: enhancement of activity of noble metal nanoparticles and their alloys by supporting or modifying. Electrochim Acta 110:474–483
12. Kulesza PJ, Faulkner LR (1993) Solid-state electroanalysis of silicotungstic acid single crystals at an ultramicrodisk electrode. J Am Chem Soc 115:11878–11884
13. Ingersoll D, Kulesza PJ, Faulkner LR (1994) Polyoxometallate-based layered composite films on electrodes preparation through alternate immersions in modification solutions. J Electrochem Soc 141:140–147
14. Makowski O, Kowalewska B, Szymanska D, Stroka J, Miecznikowski K, Palys B, Malik MA, Kulesza PJ (2007) Controlled fabrication of multilayered 4-(pyrrole-1-yl) benzoate supported poly(3,4-ethylenedioxythiophene) linked hybrid films of Prussian blue type nickel hexacyanoferrate. Electrochim Acta 53:1235–1243
15. Adamczyk L, Kulesza PJ, Miecznikowski K, Palys B, Chojak M, Krawczyk D (2005) Effective charge transport in poly (3, 4-ethylenedioxythiophene) based hybrid films containing polyoxometallate redox centers. J Electrochem Soc 152:E98–E103
16. Ernst A, Makowski O, Kowalewska B, Miecznikowski K, Kulesza PJ (2007) Hybrid bioelectrocatalyst for hydrogen peroxide reduction: immobilization of enzyme within organic–inorganic film of structured Prussian blue and PEDOT. Bioelectrochemistry 71: 23–28
17. Kowalewska B, Miecznikowski K, Makowski O, Palys B, Adamczyk L, Kulesza PJ (2007) Preparation and spectroelectrochemical characterization of composite films of poly(3,4-ethylenedioxythiophene) with 4-(pyrrole-1-yl) benzoic acid. J Solid State Electrochem 11(8):1023–1030
18. Li W, Chen J, Zhao J, Zhang J, Zhu J (2005) Application of ultrasonic irradiation in preparing conducting polymer as active materials for supercapacitor. Mater Lett 59:800–803
19. Bobacka J, Lewenstam A, Ivaska A (2000) Electrochemical impedance spectroscopy of oxidized poly(3, 4-ethylenedioxythiophene) film electrodes in aqueous solution. J Electroanal Chem 489:17–27
20. Gurunathan K, Vadivel Murugan A, Marimuthu R, Mulik UP, Amalnerkar DP (1999) Electrochemically synthesised conducting polymeric materials for applications towards technology in electronics, optoelectronics and energy storage devices. Mater Chem Phys 61:173–191
21. Du X, Wang Z (2003) Effects of polymerization potential on the properties of electrosynthesized PEDOT films. Electrochim Acta 48:1713–1717
22. Das TK, Prusty S (2012) Review on conducting polymers and their applications. Polym-Plast Technol Eng 51:1487–1500
23. Pope MT (1983) Heteropoly and isopoly oxometalates. Springer-Verlag, Berlin
24. Day VW, Klemperer WG (1985) Metal oxide chemistry in solution: the early transition metal polyoxoanions. Science 228:533–541
25. Gomez-Romero P, Casan-Pastor N (1996) Photoredox chemistry in oxide clusters. Photochromic and redox properties of polyoxometalates in connection with analog solid state colloidal systems. J Phys Chem 100:12448–12454
26. Sakmeche N, Aron JJ, Aeiyach S, Lacaze PC (2000) Usefulness of aqueous anionic micellar media for electrodeposition of poly-(3, 4-ethylenedioxythiophene) films on iron, mild steel and aluminium. Electrochim Acta 45:1921–1931
27. Song Y, Long D, Cronin L (2010) Hybrid polyoxometalate clusters with appended aromatic platforms. Cryst Eng Comm 12:109–115
28. Chaumont A, Wipff G (2008) Ion aggregation in concentrated aqueous and methanol solutions of polyoxometallates Keggin anions: the effect of counterions investigated by molecular dynamics simulations. Phys Chem Chem Phys 10:6940–6953
29. Lopez X, Miro P, Carbo JJ, Rodríguez-Fortea A, Bo C, Poblet JM (2010) Current trends in the computational modelling of polyoxometalates. Theor Chem Accounts 128:393–404
30. Muller A, Shah SQN, Bogge H, Schmidtmann M (1999) Molecular growth from a Mo_{176} to a Mo_{248} cluster. Nature 397:48–50
31. Fang XK, Anderson TM, Hill CL (2005) Enantiomerically pure polytungstates: chirality transfer through zirconium coordination centers to nanosized inorganic clusters. Angew Chem Int Ed 44: 3540–3610
32. Wu CD, Lu CZ, Zhuang HH, Huang JS (2002) Hydrothermal assembly of a novel three-dimensional framework formed by

[GdMo12O42] 9-anions and nine coordinated GdIII cations. J Am Chem Soc 124:3836–3837
33. Coronado E, Gimenez-Saiz C, Gomez-Garcıa CJ, Capelli SC (2004) Metallic conductivity down to 2 K in a polyoxometalate-containing radical salt of BEDO-TTF. Angew Chem Int Ed 43: 3021–3029
34. Nyman M, Bonhomme F, Alam TM, Rodriguez MA, Cherry BR, Krumhansl JL, Nenoff TM, Sattler AM (2002) A general synthetic procedure for heteropolyniobates. Science 297:996–998
35. Fitt: An XPS curve fitting. Fitt program with GTK library (ver. 1.2), introduced in 2000. Available from: http://www.gtk.org
36. Wagner CD, Naumkin AV, Kraut-Vass A, Allison JW, Powell CJ, Rumble JR Jr (2003) NIST X−ray photoelectron spectroscopy database NIST. Standard Reference Database 20, Version 3.5. http://srdata.nist.gov/xps
37. Rocchiccioli-Detcheff C, Fournier M, Franck R, Thouvenot R (1983) Vibrational investigations of polyoxometalates. 2. Evidence for anion-anion interactions in molybdenum(VI) and tungsten(VI) compounds related to the Keggin structure. Inorg Chem 22:207–216
38. Randriamahazaka H, Noel V, Chevrot C (1999) Nucleation and growth of poly (3, 4-ethylenedioxythiophene) in acetonitrile on platinum under potentiostatic conditions. J Electroanal Chem 472: 103–111
39. Barsukov V, Chivikov S, Barsukov I, Motronik T (1996) New promising electrochemical systems for rechargeable batteries. In: Barsukov V, Beck F (eds). Kluwer Academic, Dordrecht, p 419
40. Inzelt G, Pineri M, Schultze JW, Vorotyntsev MA (2000) Electrochim Acta 45:2403–2421
41. Rubinson JF, Mark HB, Wieckowski A (eds) (1999) Jr., in Interfacial electrochemistry, conducting polymer films as electrodes. Marcel Dekker, New York
42. Inzelt G (1994) Electroanalytical chemistry: a series of advances. In: Bard AJ (ed). Marcel Dekker, New York
43. Bergman B, Hanks TW (2000) Spectroscopic, microscopic, and surface analysis of alkanethiol- and fluoroalkanethiol-modified conducting polymer thin films. Macromolecules 33:8035–8042
44. Rocchiccioli-Detcheff C, Fournier M (1991) Catalysis by polyoxometalates. Part 3.—Influence of vanadium(V) on the thermal stability of 12-metallophosphoric acids from in situ infrared studies. J Chem Soc Faraday Trans 87(24):3919–3924
45. Tayeb KB, Lamonier C, Lancelot C, Fournier M, Payen E, Bertoncini F, Bonduelle A (2009) Preparation of new oxidic precursors based on heteropolyanions for efficient hydrocracking catalysts. C R Chimie 12:692–698
46. Allaoui LA, Aouissi A (2006) Effect of the Brønsted acidity on the behavior of CO2 methanol reaction. J Mol Catal A: Chem 259:281–285
47. Adamczyk L, Giza K, Dudek A (2014) Electrochemical preparation of composite coatings of 3, 4-etylenodioxythiophene (EDOT) and 4-(pyrrole-1-yl) benzoic acid (PyBA) with heteropolyanions. Mater Chem Phys 144:418–424
48. Adamczyk L, Kulesza PJ (2011) Fabrication of composite coatings of 4-(pyrrole-1-yl) benzoate-modified poly-3,4-ethylenedioxythiophene with phosphomolybdate and their application in corrosion protection. Electrochim Acta 56:3649–3655
49. Menom VP, Lei J, Martin CR (1996) Investigation of molecular and supermolecular structure in template-synthesized polypyrrole tubules and fibrils. Chem Mater 8:2382–2390
50. Fichet O, Tran-Van F, Teyssie D, Chevrot C (2002) Interfacial polymerization of a 3, 4-ethylenedioxythiophene derivative using Langmuir–Blodgett technique. Spectroscopic and electrochemical characterizations. Thin Solid Films 411:280–288
51. Kuhn A, Anson FC (1996) Adsorption of monolayers of $P_2M_{o18}O_{62}^{6-}$ and deposition of multiple layers of $Os(bpy)_3^{2+}$–$P_2M_{o18}O_{62}^{6-}$ on electrode surfaces. Langmuir 12: 5481–5488
52. Cheng L, Niu L, Gong J, Dong S (1999) Electrochemical growth and characterization of polyoxometalate-containing monolayers and multilayers on alkanethiol monolayers self-assembled on gold electrodes. Chem Mater 11:1465–1475
53. Cheng L, Pacey GE, Cox JA (2001) Preparation and electrocatalytic applications of a multilayer nanocomposite consisting of phosphomolybdate and poly (amidoamine). Electrochim Acta 46:4223–4228